1999

Resuspension of Particles by Aerodynamic Deagglomeration

Mark Fonda
NASA AMES RESEARCH CENTER, MS 239-4, MOFFETT FIELD, CA

Mike Petach
TRW SPACE & ELECTRONIC GROUP, APPLIED TECHNOLOGY GROUP, REDONDO BEACH, CA

C. Fred Rogers
DESERT RESEARCH INSTITUTE, PO BOX 60220, RENO, NEVADA

Judith Huntington
SETI INSTITUTE, 2035 LANDINGS DRIVE, MOUNTAIN VIEW, CA

David Stratton
SETI INSTITUTE, 2035 LANDINGS DRIVE, MOUNTAIN VIEW, CA

See next page for additional authors

Aerosol Science and Technology 30:509–529 (1999)

Published by Taylor & Francis, Inc.
0278-6826 / 99 / $12.00

Resuspension of Particles by Aerodynamic Deagglomeration

Mark Fonda, Mike Petach, C. Fred Rogers, Judith Huntington, David Stratton, Kenji Nishioka, and Mark Tipo

NASA AMES RESEARCH CENTER, MS 239-4, MOFFETT FIELD, CA U.S.A. 94035 (M. F.), TRW SPACE & ELECTRONIC GROUP, APPLIED TECHNOLOGY GROUP, REDONDO BEACH, CA U.S.A. 90278 (M. P.), DESERT RESEARCH INSTITUTE, PO BOX 60220, RENO, NEVADA U.S.A. 89506 (C. F. R.), SETI INSTITUTE, 2035 LANDINGS DRIVE, MOUNTAIN VIEW, CA U.S.A. 94043 (J. H., D. S., AND K. N.), HERNANDEZ ENGINEERING INC., NASA AMES RESEARCH CENTER, MOFFETT FIELD, CA U.S.A. 94035 (M. T.)

ABSTRACT. A deagglomerator system was developed, characterized by laboratory tests, and flown under low-gravity (low-g) microgravity conditions. Requirements for a dry powder deagglomeration system were generated by university and National Aeronautics and Space Administration (NASA) scientists from diverse fields of interest including exobiology, planetary sciences, and atmospheric sciences. Existing deagglomeration methods and devices are reviewed. An aerosol generation method suitable for dry powders over a large range of particle sizes and types at high concentrations with consistent deagglomeration efficiency are evaluated. Development of a pulsed-flow laboratory device and experimental approaches to meet the requirements without being g-dependent are described. Results of laboratory one-g quantitative characterization on one type of dry powder particle generator is discussed. Data from NASA low-g tests are summarized.

INTRODUCTION

Aerosol generation requirements often include the resuspension of particles from powder samples, i.e., from previously subdivided, solid material. Some currently-relevant examples of experimental uses for deagglomerated powder aerosols include coagulation studies involving multimodal particles, calibration of light scattering instruments, and evaluation of detection methods for diseases carried by windblown dust. Commercial devices, laboratory systems studies, and manufacturing processes resuspend and disperse various powders in gravity-dependent systems, generally using significant amounts of carrier gas during the dispersion process.

The motivation for the hardware development work which we report here originated with the stated requirements of several experiments proposed for low-gravity (low-g) research in the context of a multidisciplinary NASA program, the Gas-Grain Simulation Facility (GGSF; Huntington et al. 1994). A definition study was conducted, and an aerosol generation breadboard was built and tested. These efforts addressed a broad range of experimental requirements pertaining to researchers' interests

from fields including exobiology, planetary sciences, atmospheric sciences, and astrophysics. This development effort had the following requirements:

1. develop a dry powder aerosol generation technique that covers a range of particle sizes and types;
2. obtain high concentrations, minimizing particulate carrier gas volume requirements;
3. avoid vacuum or high temperature requirements;
4. produce a generator which is gravity and orientation independent;
5. attain consistently high deagglomeration efficiency without fracturing or damaging the particles.

Although there is extensive literature on deagglomeration, it appeared that no existing device and/or method could satisfy all of these requirements for deagglomerated solid particle aerosols. The objectives of the research reported in this paper are as follows:

1. survey existing methods, choose an approach, and build a laboratory "breadboard" device that potentially meets experimenters' requirements without g-dependence: particle sizes from < 1 to > 10 μm; concentrations from < 1 to 10^8 cm^{-3};
2. identify critical operating parameters and develop a test plan to vary them;
3. operate the system according to the test matrix and quantify the results in terms of concentration and deagglomeration efficiencies;
4. construct a low-g test platform for the evaluation of the deagglomerator and make this test platform and breadboard device available to the scientific community;
5. identify further parameters/issues to investigate.

In the following sections we describe the development effort's quantitative characterization of one type of dry powder deagglomeration particle generator. A summary of the physical factors which affect powder deagglomeration and approaches to quantifying the output are given in "Aspects of Generation." The options for deagglomeration techniques and hardware are described in "Deagglomeration Technique Selection and Hardware Development," the evaluation methodology is described in "Experimental Approach," and the one-g results are given in "Results of the One-g Deagglomerator Tests." The low-g platform and breadboard device test results are described in "Low-g Tests." The findings are summarized in "Summary."

ASPECTS OF GENERATION

Differing approaches to the generation of solid particle aerosols from powders have been developed, including various aerodynamic schemes and fluidized beds, coupled with a variety of powder feed or injection methods. These approaches have been reviewed and compared by several authors including Fuchs (1989), Hinds (1980), Hidy (1984), and John (1993). It is not always clear that the design goal of the different methodologies has been the generation of *singlet* particles, which requires total deagglomeration of the powder samples, but that is the goal of the present work.

Particle Cohesion and Adhesion

The underlying physical mechanisms and factors in powder deagglomeration are not perfectly understood. Particles are held together by short range and surface, nonretarded and retarded London-van der Waals and electrostatic forces. The short range and surface forces are strongly composition dependent, while the other forces are less so. Over-riding composition dependencies, however, is the fact that surface irregularities and morphological variations make it difficult to estimate the variations in separation distance and surface area of contact, of agglomerated particles. Thus it is difficult to apply or even verify theoretical estimates of the attractive forces which must be overcome in accom-

plishing the deagglomeration of particles (Hidy 1984).

In general, existing devices apply two types of forces to agglomerated particles in order to separate them: aerodynamic and vibrational (the latter in fluidized beds). The common experience that small particles are harder to separate than larger ones is supported by theory. This relatively simple picture can, however, be greatly modified by the presence of electrostatic charge and/or condensed fluids. Because of the difficulties inherent in quantifying particle electric charge before, during, and after deagglomeration, published studies have not characterized deagglomeration efficiencies as a function of this parameter; the results published in this paper are based on dry, nonconducting particles and carrier gas for which electric charge effects are expected to be significant. The published literature on deagglomeration methods can be viewed from two perspectives, which are necessary in order to undertake any advancement in the quantitative understanding of such methods: first, what are the parameters and design factors which exert significant effects on the operation of deagglomerators; and second, what are the quantities necessary to characterize the output particle distributions produced by deagglomerators.

Operation of Deagglomerators

The parameters and variables which control the operation of deagglomerators understandably differ between the fluidized bed and aerodynamic approaches. Parameters unique to fluidized beds include the size and composition of the glass or metallic bed particles, the depth of the bed, and the presence or absence of deliberately induced mechanical vibrations in the bed (Iinoya and Masuda 1980; John 1993). Aerodynamic methods rely on viscous and pressure forces induced in velocity shear zones, and hence unique to these methods are parameters which determine the geometrys of the shear zones, such as the widths of slits or the diameters of passages through which the sample is forced to flow (Eadie and Payne 1954; Fuchs 1989; Fuchs and Selin 1964). Other controlling parameters include the powder feed method and the carrier gas flow.

First, the method of feeding or injecting the powder sample affects the performance of both types of devices. Fluidized beds are operated with mechanical feeders such as moving chains (Hinds 1980) and occasionally without feeders in a batch mode (John 1993). Apart from clogging or failure of the chain feed, the main concern with fluidized bed feeders appears to be that of consistently and uniformly distributing the powder at the bottom of the bed. Iinoya and Masuda (1980) show some evidence for reduced deagglomeration efficiency of a fluidized bed as the powder feed rate is increased.

Hinds (1980) describes several of the feed mechanisms developed for various aerodynamic deagglomerators, for which the main criterion seems to be providing constant mass fluxes at a given setting, but which can be reset for best results. These methods feed controlled amounts of powder to carrier flows or impinging gas jets in a variety of aerodynamic devices.

Second, the efficiencies of both deagglomeration approaches tend to depend on carrier gas flows. In fluidized beds, the carrier gas flow lifts the bed particles along with the sample particles and generates both motion and collisions of the bed particles and aerodynamic forces on the sample particles (Hinds 1980; Hidy 1984). Increasing fluidization velocities enhance deagglomeration for most, but not all, powder types in a fluidized bed (Iinoya and Masuda 1980). In aerodynamic devices, the carrier flow may directly generate the velocity shear which separates the agglomerates or it may merge with additional flows before the final velocity distribution is generated. Reducing carrier air flows in aerodynamic deagglomerators increases the powder mass/carrier gas volume ratio, which appears to adversely affect deagglomeration efficiency (Iinoya and Masuda 1980).

A heuristic explanation for the dependence of deagglomeration performance on particle number concentration in a shear based device is as follows. The shear in the deagglomerator slit due to the gas velocity gradients is the fundamental mechanism for breaking apart the aggregates. The particle velocity differences that result from the gas velocity gradients also cause particles to come together, however, resulting in agglomeration. Thus the deagglomeration performance of the device is a balance between deagglomeration and re-agglomeration. The deagglomeration term is increased by increasing the shear, which unfortunately also increases the reagglomeration term. A similar situation also exists with the particle residence time in the deagglomerator. The deagglomeration term is increased by increasing the residence time since sufficient time must be allowed for the location and orientation of the aggregates in the shear field to vary over their passage through the slit such that they pass through a shear maximum. However, an increase in residence time also allows more time for particles to "catch up" with one another. The only variable which does not increase both terms simultaneously is the particle spacing, i.e., the particle number concentration. The farther apart the particles are initially, the less likely they are to be brought together. Thus, reducing the particle number concentration does nothing to enhance the fundamental ability to deagglomerate particles, but it does diminish the fraction of particles that are reagglomerated.

Iinoya and Masuda (1980) showed, experimentally and theoretically, that the deagglomeration performance of a device based on shear is approximately given by the expression

$$\left(D_o/D_i\right)^3 = \left(A/B\right)n_i + e^{(-A\,t)}, \qquad (1)$$

where

- D_o is the output mass median particle diameter,
- D_i is the fully deagglomerated mass median diameter,
- A is the dispersion (deagglomeration) constant,
- B is the agglomeration constant,
- t is the mean residence time in the deagglomerator, and
- n_i is the initial particle number concentration,

which illustrates the points in the discussion above. When the deagglomeration data are plotted as $\left(D_o/D_i\right)^3$ versus n_i, the intercept and an estimate of the residence time can be used to determine the deagglomeration constant "A." The slope then shows the relative relationship between deagglomeration and reagglomeration.

Deagglomerator Output Characterization

The deagglomeration "efficiencies" of fluidized beds, aerodynamic deagglomerators, and other methods have been evaluated both by using size measuring instruments, such as optical particle counters and impactors (e.g., Iinoya and Masuda 1980), and by applying electron or light microscopy (e.g., Fuchs and Selin 1964; Fuchs and Murashkevich 1970). Reductions in overall size distribution parameters such as the mass median diameter are interpreted as evidence that agglomerates are being broken down into singlet constituent particles. A problem with utilizing optical counter data in this way is that doublets, triplets, or low-order multiples may not be resolved from singlets for polydisperse powders. In the approach of Fuchs and Selin (1964) and Fuchs and Murashkevich (1974), manual microscopy is applied and particles are inventoried according to the number of constituent particles which are observed. The deagglomeration efficiency E is then defined as the ratio of the number of singlet particles to the total number of particles:

$$E = N_1/\left(N_1 + 2N_2 + 3N_3 + \ldots\right), \qquad (2)$$

where N_n is the number of agglomerates containing n particles.

In addition to the deagglomeration efficiency, a critical measure of deagglomerator output is the particle mass concentration, which is the ratio of powder sample mass to carrier gas volume, evaluated at ambient pressure. The mass concentration converts directly into the particle concentration delivered by the deagglomerator (prior to any dilution) if the distribution of singlets, doublets, etc., is known. Hinds (1980) summarizes the findings pertinent to several deagglomeration methods and indicates that the undiluted mass concentrations range up to about 150 g/m^3. As noted above, the mass concentration is also an input factor which seems to affect the efficiency of aerodynamic deagglomerators.

DEAGGLOMERATION TECHNIQUE SELECTION AND HARDWARE DEVELOPMENT

Experimenters interested in long-duration aerosol studies (e.g., coagulation) may eventually be able to utilize low-g platforms such as the Space Shuttle or Space Station. For this reason, gravity-independent deagglomeration techniques were sought, ruling out fluidized beds or other approaches which rely on gravity to confine the sample powder to a specified location. Aerodynamic deagglomeration approaches were reviewed, and a method which had previously shown potential for efficient deagglomeration at high mass concentrations was chosen for further study. Fuchs and Selin (1964) and Fuchs and Murashkevich (1970) report work on the characterization of aerodynamic powder deagglomerators of two designs: first, a closely-matched male and female cone pair which when assembled, provides a conical annular gap; second, a simple tubing coil. In each device, lateral velocity gradients produce shear, which is hypothesized to provide the forces needed for deagglomeration. The fractions of singlet, doublet, triplet, etc., particles were determined by microscopy as a function of flow velocity. Deagglomeration efficiencies up to 1.00 (ratio of singlets to all particles, determined as in Equation (2)) were obtained, but the description of the operating parameters is extremely brief. The matched cone idea apparently originated with work of Eadie and Payne (1954), who reported its application to a method of determining dry powder size distributions based on the fall velocities of the deagglomerated powders in a sedimentation column. Because the matched cone method seemed better suited to high mass concentration throughput, it was selected for this investigation.

Rajathurai et al. (1990) report successful powder deagglomeration and dispersion with a shock and expansion wave-driven method; this research was not known to us at the initiation of the work reported here. These experiments involved shock and expansion waves created when pressurized gas ruptured a diaphragm. This approach worked well, with high deagglomeration efficiencies, for submicron (0.2–0.5 μm count median diameter) quartz and polystyrene latex particles. The research reported by Rajathurai et al. (1990) is quite beneficial in terms of elucidating sonic aerodynamic deagglomeration mechanisms, which are also involved in our approach; however, the method we adopted seems to have at least two significant advantages when compared to the Rajathurai et al. (1990) method: first, the carrier gas is explicitly controlled and minimized; second, the physical arrangement is amenable to repeated rather than "single-shot" experiments.

The experimental arrangement used in the work reported here is based on the matching cones arrangement of Eadie and Payne (1954) and Fuchs and Selin (1964). In the earlier work by these investigators, there was no attempt to provide a controlled powder dilution system and only a brief exploration of the effects of cone gap width and air velocity on the deagglomeration efficiency was performed. The present deagglomerator system (Figure 1) has evolved to include a powder sample holder, concentration control, deagglomerator, a test chamber, and instrumentation control circuits. This system minimizes carrier gas volume by using brief, pulsed flows.

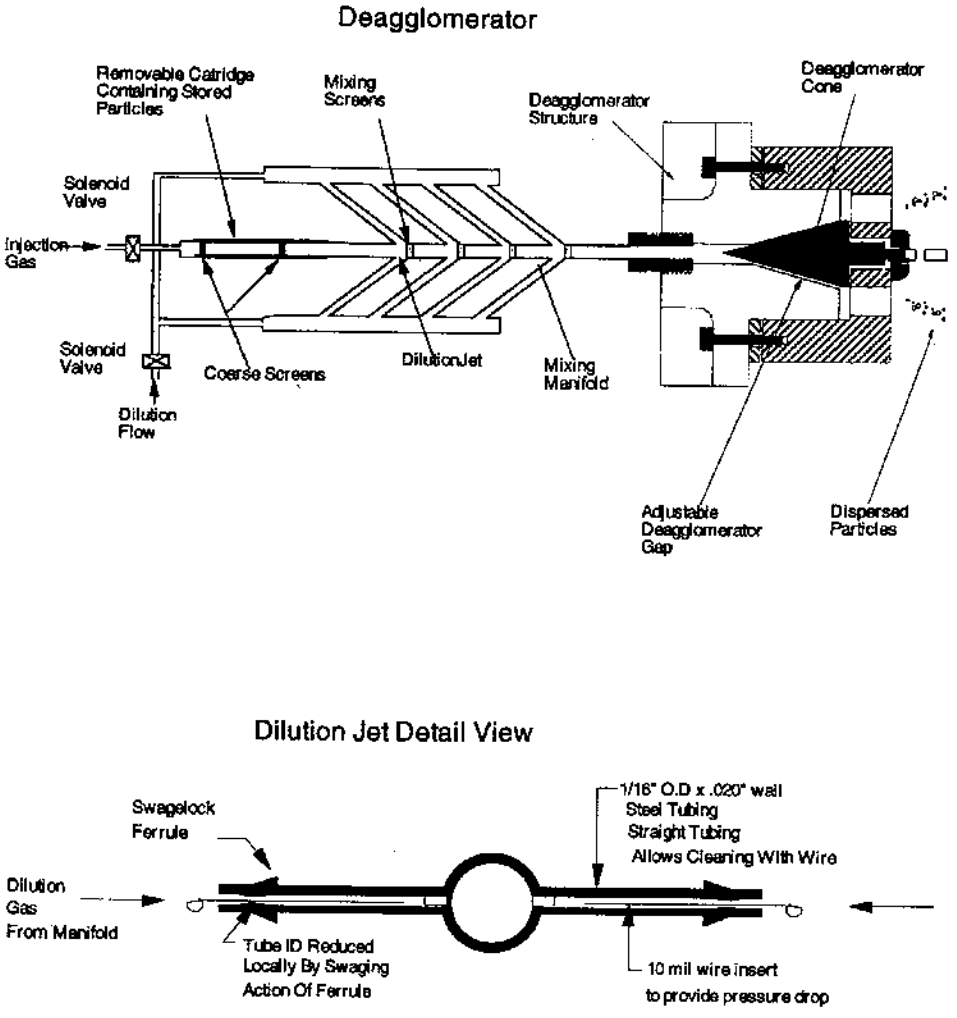

FIGURE 1. Deagglomerator drawing.

Sample Holder

The sample holder consists of a 3.6 cm long section of aluminum tube with an inner diameter of approximately 0.3 cm. This tube is terminated at one end with a connection to a tee. There is a 400 mesh stainless steel screen sandwiched between two 80 mesh screens at the junction between the tube and the tee. These screens hold the powder in the tube as the powder is poured into the opposite end of the tube to form a cylindrical plug of loosely packed dust. Although the openings in the 400 mesh screen are larger than the particle diameters, the powder cohesion allows the powder to bridge the openings. The mass of dust determines the height to which the dust plug fills the tube. The length of the powder holder tube can accommodate up to 200 mg of powder sam-

ple; typically experiments have been conducted with amounts of 85 mg. Once loaded into the tube, powder can be lightly tamped. In this state the powder will remain as a dust plug when the tube is put into a horizontal position. The open end of the sample holder mates to the dilution section via a connecting fitting which can be disconnected and reconnected to allow the manual powder loading procedure. The screened inlet end of the sample holder connects to a solenoid valve which controls the timing of the gas flow that dispenses the powder.

Dilution Flow

The concentration control system consists of four pairs of opposed jets that inject dilution gas into the main flow. The jet tubes are connected to a manifold carrying dilution gas from the dilution flow solenoid valve. Each pair of opposed jets consists of a union with two pieces of 0.16 cm tubing penetrating the opposite walls at approximately 20 degrees. Thick wall (0.05 cm) tubing was used to obtain a high intrinsic pressure drop and to keep the velocity in the tubes high. The ferrules on the 0.16 cm tubing were purposely over-tightened to swage down the tube inner diameter locally; this local restriction was then able to be further constricted to various degrees by inserting wires of different diameters. The union containing each opposed jet pair is followed by a 3.18 cm long section of 0.32 cm inner diameter aluminum tubing to promote mixing. There is an 80 mesh steel screen across the tube at the exit of each union, again to promote mixing.

Deagglomerator

The deagglomerator section (Figure 1) consists of a pair of concentric cones with an adjustable gap, or slit width, between the cones. The dimensions of the cones are approximately the same as reported by Eadie and Payne (1954). Insert rings of different thicknesses are used to set the deagglomerator slit widths; 39, 79, 118, and 145 μm slit widths are used in the tests reported here. The pressure drops obtained with this system using 0.025 cm diameter wires and a 79 μm slit width are shown in Figure 2.

The operating range of the dilution flow can be read from this figure for a given desired deagglomeration pressure. The range of dilution pressure settings that can be used for a 4.1×10^5 Pa, 60 psig, deagglomerator setting are illustrated in Figure 2 by the arrows. Dilution gas flows are limited on the low end since the dilution flow manifold pressure must be greater than the required deagglomeration pressure. High dilution gas flows are limited by the mixing plenum chamber pressure which must be lower than the deagglomeration pressure. A different set of dilution flow pressure setting ranges will result from the different back pressures produced at different slit widths and with different inserts in the dilution jets. The operating ranges for slit widths of 40 and 118 μm were similarly derived. Figure 3 shows the steady-state gas flow rates as a function of the upstream pressure for the four deagglomerator slit widths. For example, a typical experiment involving a 1-s gas pressure pulse at 4.1×10^5 Pa (60 psig) would result in about 2 L (at standard conditions) of gas in addition to the particles injected into the chamber.

The control circuit provides the timing for the opening of the two solenoid valves on the deagglomerator, and it provides a signal for timing reference or for triggering a data acquisition system. The delay and duration of the opening of each solenoid valve can be independently set.

The deagglomerator diagnostic instrumentation consists of two pressure transducers for monitoring the pressures in the deagglomerator and dilution control sections and three laser/detector pairs for monitoring particle concentration at the exit plane of the deagglomerator. The pressure transducers are miniature flush-mount strain gauge-type pressure transducers with submillisecond response and a range of $0–1.73 \times 10^6$ Pa (0–250 psig). The pressure transducers are mounted into the bodies of each

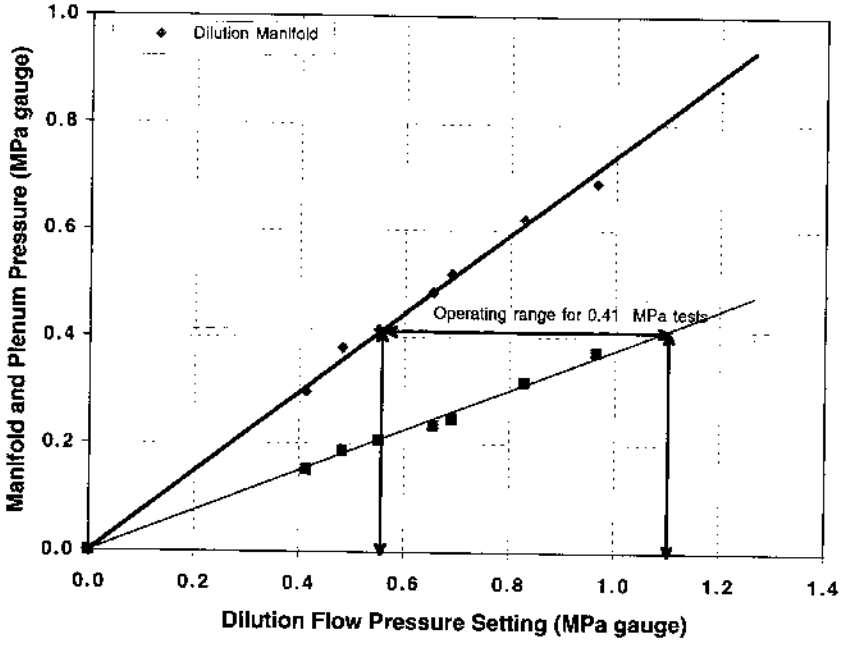

FIGURE 2. Dilution flow pressure settings.

solenoid valve on the downstream side of the valve.

The lasers are InGaAlP laser diodes, which provide approximately 3 mW at 670 nm. The lasers have been mounted in aluminum standoffs such that the three laser/detector pairs form a plane approximately 7.5 cm downstream of the deagglomerator exit. The detectors are large area silicon photodiodes.

EXPERIMENTAL APPROACH

The experiments were conducted according to a test matrix which prescribed measurements of the deagglomeration efficiencies at three slit widths, three gas pressures, and three particle concentrations using dry 5–10 μm size classified Arizona Test Dust (Powder Technology Inc., Burnsville, MN). Nearly monodispersed particles were used in all tests in order to vary one parameter at a time. More limited tests were also conducted with dry monodisperse 10 μm and 2 μm glass microspheres (Duke Scientific Corp., Palo Alto, CA) at the optimum slit width, pressure, and exit plane concentration as determined by the results with the Arizona Test Dust.

There are many other parameters which potentially effect the deagglomeration performance of the system but which were not explicitly defined during the discussions that lead to the test matrix. A short summary of the most relevant of these follows.

1. The Arizona Test Dust was prepared in an oven at 150°F to insure a completely dry state, or at least a uniform moisture content during the course of testing.
2. The gas used was nitrogen produced from the boil-off of liquid nitrogen and repressurized. The relative humidity of this gas was

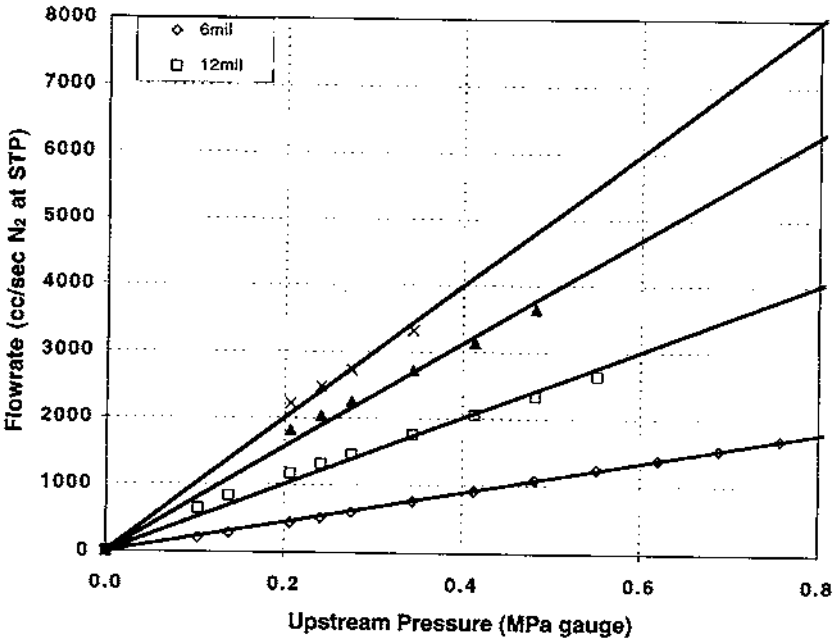

FIGURE 3. Deagglomeration flowrate versus pressure.

not measured but it was assumed to be essentially zero.

3. All tests were done with the deagglomerator discharging into a test chamber filled with ambient laboratory air, i.e., a chamber pressure of 1 atm.
4. No attempts at charge neutralization were made either to the gas entering the system or to the dusty gas exiting the deagglomerator.
5. The deagglomerator materials (brass, steel, aluminum, etc.) were held constant throughout the testing. No attempts were made to choose materials which minimize triboelectric effects nor was any attempt made to estimate triboelectric effects. The deagglomeration efficiencies are conservative as regards charge effects; if conducting powders were utilized, it is expected that the deagglomeration efficiencies would increase.

The laboratory setup utilized a 170 L cylindrical chamber 60 cm in diameter and 60 cm in length. The deagglomerator was mounted above the chamber, discharging downwards. A particle sampling filter was located at the center of the bottom of the chamber. The dispersed dust jet passed through laser beams which were used to determine the deagglomerator exit-plane concentration history.

Pressure Settings

The pressure history data for each test were obtained from the pressure transducers described earlier. The data were recorded on a computer-based data acquisition system for subsequent display and analysis. The timing of the gas flows was controlled by the deagglomerator solenoid valves described earlier. The flow to the dilution manifold was initiated first to allow the manifold to come up to full pressure. Approximately 100–200 ms later the powder sample transport flow solenoid valve was opened. Both valves were left open for approximately 1 s. The trans-

port flow solenoid was shut off first, followed by the dilution jet flow. This order was chosen so that there was no chance of driving dust into the dilution flow manifold. A typical pressure trace is shown in Figure 4, along with the resulting laser transmission trace. The total gas flow duration was purposely set to be far longer than was required to dispense the dust in order to thoroughly flush the deagglomerator system.

The Arizona Test Dust mass loaded into the sample holder was measured using an analytic balance with a resolution of 0.1 mg. The empty sample holder was tared, then filled with dust until the desired dust weight was obtained. After the desired weight of powder had been loaded, the sample holder was held in a vertical position and the sample was lightly tamped to insure that the powder was present in the form of a plug. Some posttest weights of the sample holder were obtained and compared to the pretest empty sample holder weight to determine the mass of dust remaining in the sample holder, but this was discontinued when no significant masses were measured (< 1% of the initial stored powder mass).

Laser Transmission Data

The peak exit plane concentration was inferred from the laser transmission signals measured 7.5 cm downstream of the deagglomerator slit exit. Three laser beams formed a plane perpendicular to the flow exiting the deagglomerator. The multiple beams allowed the uniformity of the dust concentration around the annulus to be estimated so that an average spatial concentration could be determined.

In the ideal case, the dust concentration could be found directly from the laser transmission signal using Beer's Law in the following form:

$$C_m = -(2\rho D_{32}/3Q_e L)\ln(I/I_0), \quad (3)$$

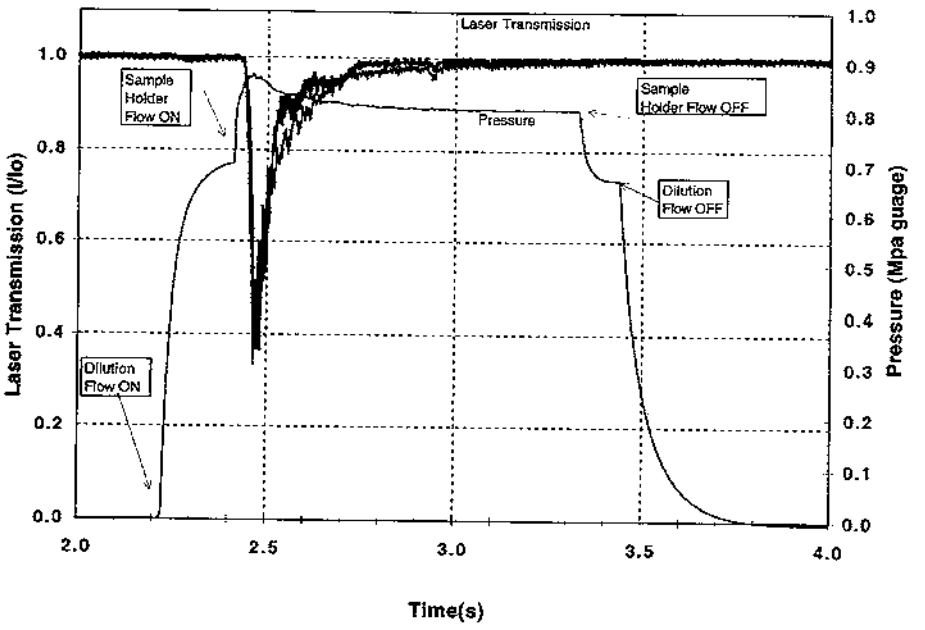

FIGURE 4. Time history of laser transmission and pressure signals.

where

C_m is the mass concentration (g/cm^3),
ρ is the particle density (g/cm^3),
D_{32} is the Sauter (or Surface Weighted) Mean Diameter (cm),
L is the optical path length (cm),
Q_e is the extinction efficiency (= 2 for this diameter and wavelength),
I/I_o is the transmitted divided by incident intensity;

since all the terms in the grouped term $(2\rho\ D_{32}/3\ Q_e\ L)$ on the right side of the equation would be known. In the present case though, all the terms can be estimated accurately except the path length. The laser beams cross an annular jet in which the concentration is probably not nearly uniform along the beam path, so it is not clear what equivalent path length to use (or how to integrate along the beam path).

An order-of-magnitude estimate for the path length can be obtained by assuming that the dust uniformly fills in the cone defined by the extension of the 15 degree half-angle deagglomerator cone out from the end of the cone (where the diameter is approximately 2 cm) to the laser beam location (7.5 cm beyond the end of the pintle), where the diameter is approximately 5 cm. In that case, assuming fully deagglomerated PTI dust, the values

ρ = 2.5 gram/cm^3,
D_{32} = 7×10^{-4} cm (determined independently),
L = 5 cm,
Q_e = 2 for these diameters and wavelength

yield a conversion equation of

$$C_m = -(1.2 \times 10^{-4}) ln(I/I_0)\ \text{g/cm}^3. \qquad (4)$$

A potentially more accurate estimate was obtained by integrating the laser transmission signals in the form $-ln(I/I_o)$ over the duration of the flow (Figure 3). Using an analogy in which the dust/gas mixture is treated as a very dense pseudogas, a mass balance shows that the total mass passing a point is obtained by integrating the product of the pseudogas "density" and volumetric flow rate over time. The pseudogas volumetric flow rate can be assumed to be equal to the clean gas volumetric flow rate and constant over the test duration. The pseudogas "density" due to the dust is given by the expression $-K\ ln(I/I_o)$, as shown above. Since the lasers only respond to the dust phase of this pseudogas, the coefficient K can be obtained by equating the integration equal to the total dust mass stored and ignoring the density of the gas. This procedure was carried out for a variety of test conditions, yielding values of K from 7.4×10^{-4} to 3.6×10^{-4} with an average value of 5.0×10^{-4} g/cm^3 , or

$$C_m = -(5.0 \times 10^{-4}) ln(I/I_0)\ \text{g/cm}^3. \qquad (5)$$

This result is higher than the order of magnitude estimate, as would be expected if the effective path length was shorter than the full diameter of the jet due to its annular geometry. The factor of 4 increase corresponds to an effective path length of 1.25 cm. This can be interpreted as meaning that the dusty jet at the laser beam location is 100 times its width at the deagglomerator cone exit (approximately $2 \times 80\ \mu$m or 1.6×10^{-2} cm), but has not quite expanded to fill the inner and outer portions of the apparent conical jet. The value obtained by the integration technique is considered to be more accurate than the order of magnitude estimate and was used to provide a conversion from relative concentration to absolute concentration in the data presentation and analysis.

Filter Sampling

The deagglomeration performance was determined using microscopic examination of particles sampled from the chamber. An open face 47 mm Nuclepore (Costar, Inc., Cambridge, MA) filter mounted in a holder at the bot-

tom of the chamber sampled the partially diluted ("farfield") particle cloud produced by the solid particle generator. Flow field visualization showed that the dust/gas cloud impinges on the far wall of the chamber within approximately 1 s and at that time has expanded to approximately 10 times its initial diameter. Thus, the dispersed dust has had little time to agglomerate and has been diluted by entrainment. The Nuclepore filters did not have air drawn through them, since this was found to produce an undesirably high concentration of particles on the filter, leading to potential coincidence errors. The natural impingement and sedimentation that resulted from the solid particle generator jet were found to produce filter exposures with 5–20 diameters between closest particles. This method of collecting particle samples follows closely the technique used by Fuchs and Selin (1964). The Nuclepore filters were covered after approximately 15–30 seconds in order to prevent reagglomerated particles from the dust cloud still circulating in the chamber from settling on the filter. The filters were then removed and examined under an optical stereo microscope to determine the degree of deagglomeration. The microscope used for these tests was a Lietz LaborLux 12HL with 10x/18 eyepieces and 20x/0.30 Dark-Field (DF) objective. DF lighting with random polarization was found to be optimum. A custom grid was made for the field stop of the ocular which divided the field of view into 6 horizontal strips, making it easier to keep track of which particles had been counted. The particles were counted and classified according to the number of individual particles (with a minimum of one) within each "aggregate." Particle counting and classification was done using the numeric keypad of a computer to enter the data into a program that recorded the data. Typically, 1000 or more aggregates were counted for each test from randomly selected locations on the filter (with a step-wise progression to prevent the possibility of repeating a location) in order to get a statistically significant estimate of the distribution tails.

RESULTS OF THE ONE-G DEAGGLOMERATOR TESTS

Deagglomeration efficiencies were evaluated in 36 tests using the 5–10 μm Arizona dust, two tests using the monodisperse 10.2 μm glass microspheres, two tests using 2.1 μm glass microspheres, and are summarized in Table 1. Deagglomeration data were obtained for the test dust at 2.1, 4.1, and 8.3 $\times$ 10^5 Pa (30, 60, and 120 psig) pressure using 39, 79, and 118 μm slit widths and varying the concentration from approximately 1 $\times$ 10^{-4} gram/cm^3 to approximately 15 $\times$ 10^{-4} grams/cm^3 with at least three concentrations for each pressure and slit width. Additional data was obtained at 7.6 $\times$ 10^4 Pa (11 psig) and 79 μm to investigate the effect of unchoked flow. Two tests were explicit repeats of one of the test conditions. The glass microsphere tests were done at 8.3 $\times$ 10^5 Pa and a slit width of 79 μm, based on results with the test dust. The deagglomeration efficiencies were calculated according to Equation (2).

Example Arizona dust deagglomeration data are presented graphically in Figures 5–8 as deagglomeration versus concentration for each slit width setting and pressures of 4.1 and 8.3 $\times$ 10^5 Pa. Additional data were obtained for a range of concentrations, all slit widths, and the remaining pressure settings to complete the test matrix. There are two reasons for presenting the data this way, which is similar to the approach of Iinoya and Masuda (1980). First, the pressure and slit width settings were easy to preset and hold constant, whereas the concentration was not able to be preset. Curve fitting of the data in this form, however, allows this data to be cross plotted along lines of constant concentration. A linear regression curve fit was used for this purpose, and the best fit line is shown on each plot. Second, this allows the data to be extrapolated to zero concentration. The extrapolation to zero concentration indicates the maximum performance available for a given slit width, pressure setting, and dust type, as previously discussed.

TABLE 1. Deagglomerator performance summary for one-g laboratory tests.

Test ID	Deagglomerator Slit Width (um)	Peak Pressure (Pa)	Average Extinction Peak (-ln(I/I0))	Dilution Pressure Setting (Pa)	Push Pressure Setting (Pa)	Dilution Insert (mils)	Total Particle Count	Deagglomeration Efficiency
ggs2	79	7.58E+04	0.751	1.03E+05	8.27E+04	na	1624	0.41
ggs3	79	8.27E+04	0.229	1.38E+05	8.27E+04	na	1424	0.50
gg12	79	2.07E+05	0.715	4.14E+05	2.07E+05	na	1341	0.68
gg13	79	2.07E+05	0.445	5.10E+05	2.07E+05	na	1153	0.78
gg14	79	2.07E+05	0.157	5.38E+05	2.07E+05	na	1081	0.80
gg15	79	2.07E+05	0.309	5.24E+05	2.07E+05	na	1222	0.74
ggs8	79	3.65E+05	0.836	4.14E+05	4.14E+05	na	1012	0.79
ggs1	79	4.00E+05	0.452	6.21E+05	4.14E+05	na	1023	0.83
84mgb	79	3.72E+05	0.357	6.21E+05	4.14E+05	na	888	0.80
ggs4	79	4.27E+05	0.141	6.55E+05	4.14E+05	na	1022	0.92
gg11	79	4.14E+05	0.901	6.55E+05	4.14E+05	10	1186	0.75
gg10	79	4.14E+05	0.211	1.03E+06	4.14E+05	10	1106	0.86
gg09	79	4.14E+05	2.625	9.65E+05	4.96E+05	na	757	0.51
ggs5	79	8.41E+05	0.252	1.38E+06	8.27E+05	10	1157	0.94
ggs6	79	7.93E+05	0.423	1.17E+06	8.27E+05	10	657	0.91
ggs7	79	7.58E+05	1.206	8.27E+05	8.27E+05	10	1154	0.78
gg16	39	4.14E+05	0.779	8.27E+05	4.14E+05	17	1371	0.83
gg17	39	4.14E+05	1.173	5.17E+05	4.69E+05	17	1427	0.65
gg18	39	4.14E+05	0.671	6.90E+05	4.27E+05	17	1299	0.73
gg19	39	4.14E+05	0.091	1.24E+06	4.14E+05	17	1051	0.92
gg20	39	2.07E+05	0.927	2.76E+05	2.21E+05	17	1247	0.69
gg21	39	2.07E+05	0.423	3.79E+05	2.21E+05	17	1190	0.78
gg22	39	2.07E+05	0.229	4.69E+05	2.07E+05	17	1046	0.81
gg24	39	8.27E+05	1.007	1.65E+06	9.10E+05	17	1184	0.78
gg25	39	8.27E+05	0.195	1.10E+06	8.41E+05	10	1135	0.84
gg26	39	8.27E+05	1.196	9.65E+05	8.41E+05	10	1263	0.77
gg27	118	4.14E+05	1.176	7.58E+05	5.17E+05	10	1578	0.78
gg28	118	4.14E+05	0.648	1.03E+06	4.34E+05	10	1790	0.79
gg29	118	4.14E+05	0.574	1.24E+06	4.14E+05	10	1176	0.85
gg30	118	4.14E+05	0.33	1.31E+06	4.14E+05	10	1173	0.85
gg31	118	2.07E+05	0.767	6.14E+05	2.07E+05	10	1311	0.74
gg32	118	2.07E+05	0.387	6.90E+05	2.07E+05	10	1131	0.80
gg33	118	2.07E+05	1.393	3.79E+05	2.21E+05	10	1395	0.65
gg34	118	8.27E+05	0.943	1.52E+06	8.62E+05	na	1722	0.72
gg35	118	8.27E+05	0.794	1.52E+06	8.62E+05	na	1324	0.72
gg36	118	8.27E+05	0.319	1.93E+06	8.27E+05	na	1807	0.76
gg37	118	8.27E+05	0.227	2.21E+06	8.27E+05	na	1380	0.77
gg38	79	8.27E+05	0.465	1.45E+06	8.27E+05	na	1510	0.87
gg39	79	8.27E+05	0.454	1.45E+06	8.27E+05	na	1503	0.89

Notes: 1. Dust sample masses were 85 +/− 1 milligram for all tests.

The vertical axis shows percent deagglomeration (Equation (2)) as determined using the optical microscope. An accuracy of +/− 5% has been assigned to these measurements, based on the spread in the data obtained with similar conditions. The horizontal axis shows the relative dust concentration at the exit plane as measured by the three laser beams. The data obtained from each of the laser beams is shown, and the deagglomeration performance is plotted at the location of the average of the three beam's data. The approximate absolute particle mass concentration for a relative concentration value of $-ln(I/I_o) = 1$ is also indicated on the horizontal axes so that approximate absolute concentrations can be obtained for all the data.

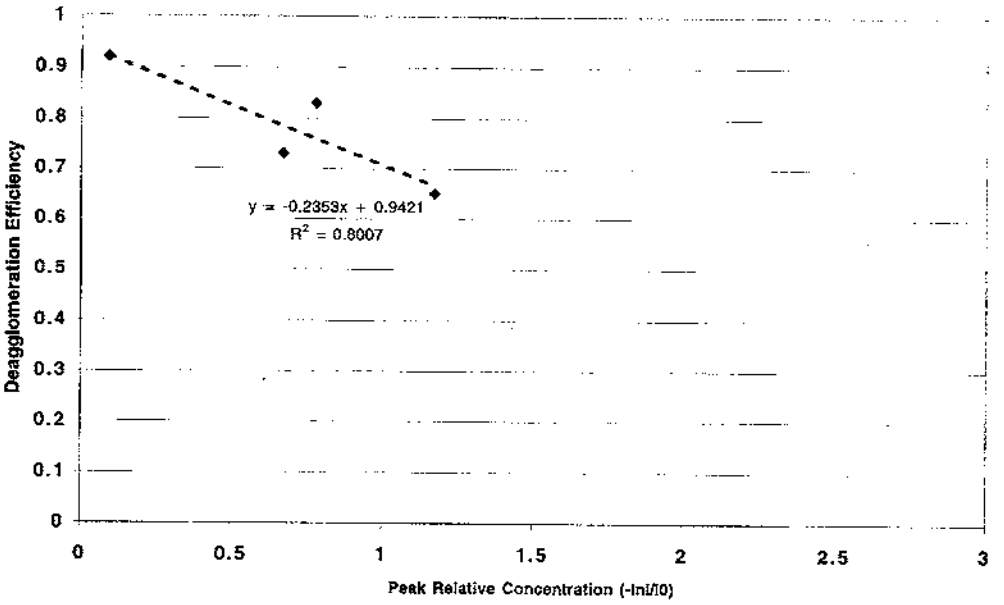

FIGURE 5. Deagglomeration efficiencies for 39 micron slit at 4.1×10^5 Pa peak pressure.

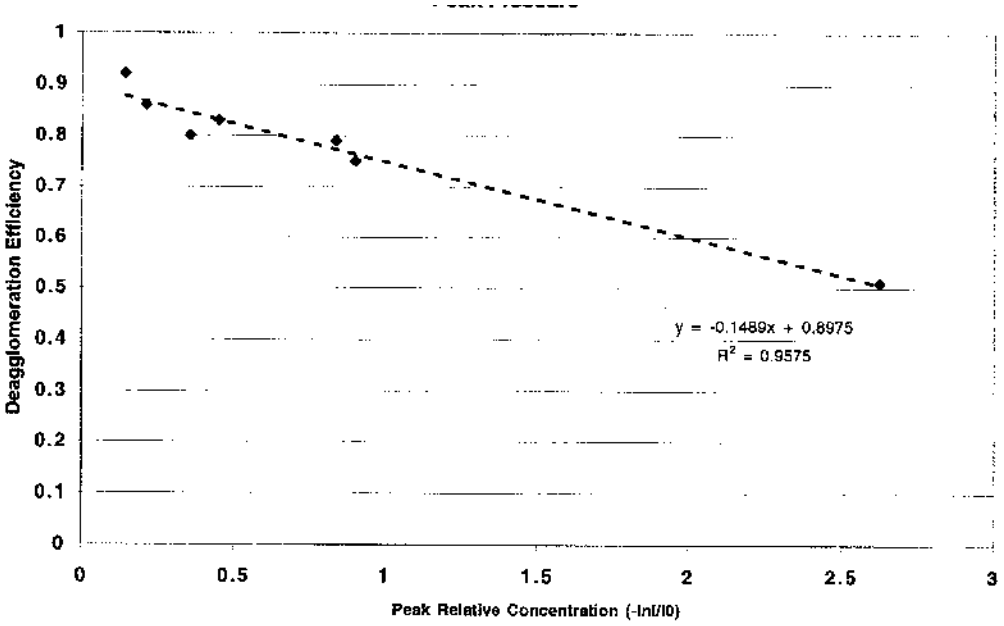

FIGURE 6. Deagglomeration efficiencies for 79 micron slit at 4.1×10^5 Pa peak pressure.

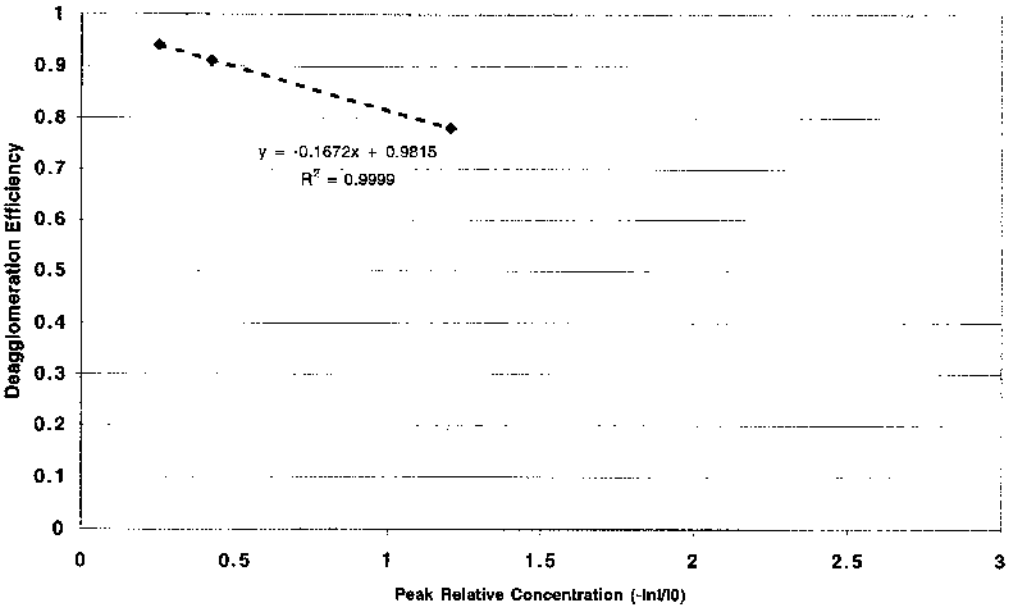

FIGURE 7. Deagglomeration efficiencies for 79 micron slit at 8.3×10^5 Pa peak pressure.

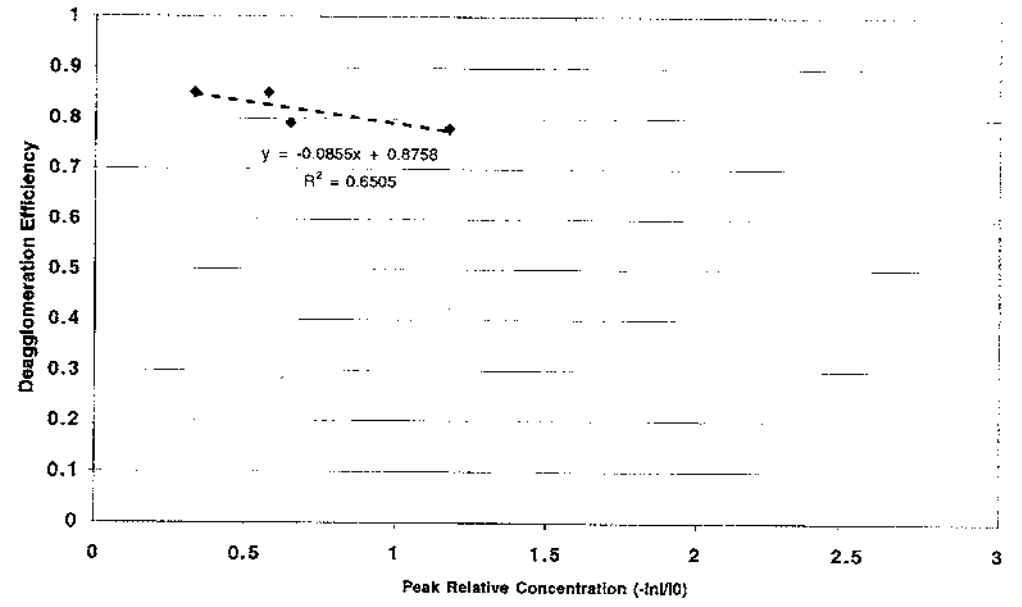

FIGURE 8. Deagglomeration efficiencies for 118 micron slit at 4.1×10^5 Pa peak pressure.

Cross plots of the data as deagglomeration versus pressure at constant slit width and constant concentration are shown in Figures 9–10. The exit plane concentrations that were chosen were the extrapolation to zero g/cm^3 and the interpolation to 2.5×10^{-4} g/cm^3 $\left(-ln\left(I/I_o\right) = 0.5\right)$. The choice for the interpolated concentration value to use for the cross plots was simply to illustrate the pressure and slit width trends at a convenient low-concentration operating point. Similar cross plots could be constructed at any other concentration in the range tested.

On these cross plots, a comparison of the data obtained at the different pressures with the 79 μm gap shows that there is a significant difference between the choked (2.1, 4.1, and 8.3×10^5 Pa) and the unchoked conditions (7.6×10^4 Pa). This would be expected since in the choked cases the flow goes supersonic in the converging section. There is a much less pronounced difference among the choked condition cases that were tested. The data obtained at the different pressures with the 39 and 118 μm gaps indicate that the deagglomeration performance increases as the pressure is raised from 2.1 to 4.1×10^5 Pa, as would be consistent with the increase in shear, but then levels off or even decreases slightly as the pressure is raised from 4.1 to 8.3×10^5 Pa. There was very little difference in deagglomeration performance between the three slit widths that were chosen. The difference between the slit widths typically falls within the data scatter of the individual data points used to make the cross plots.

Two tests (test #gg38 and #gg39) were performed as explicit repeats of an existing test dust data point (test #gg06) to characterize the device's repeatability. Both the concentration achieved and the degree of deagglomeration achieved fall within the uncertainty of the existing data point. The three data points lie within a 5% spread in deagglomeration and within a 15% spread in exit-plane concentration. Two additional tests were performed using 10.2 μm

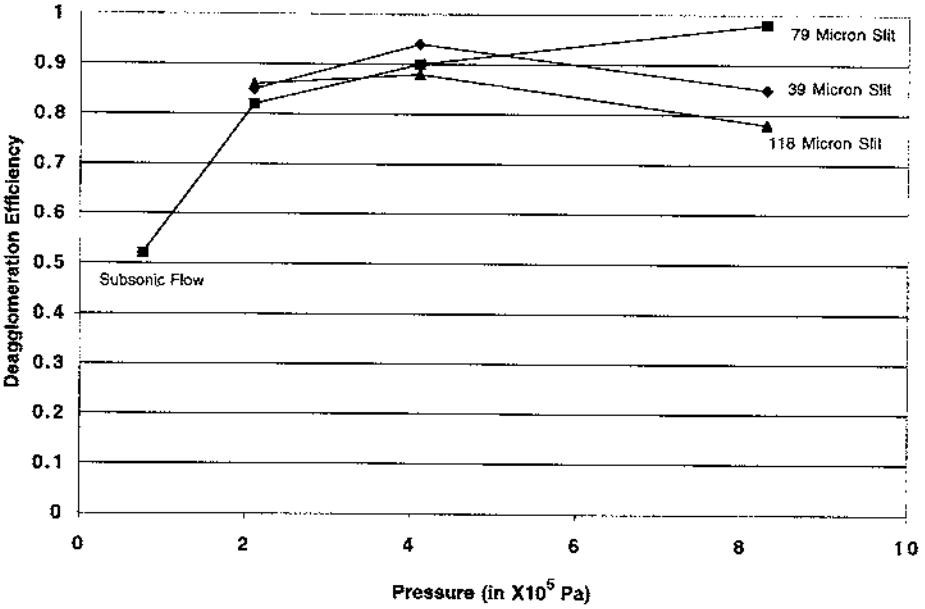

FIGURE 9. Deagglomeration efficiency versus pressure for three slit widths and $Ln\left(I/I0\right) = 0$.

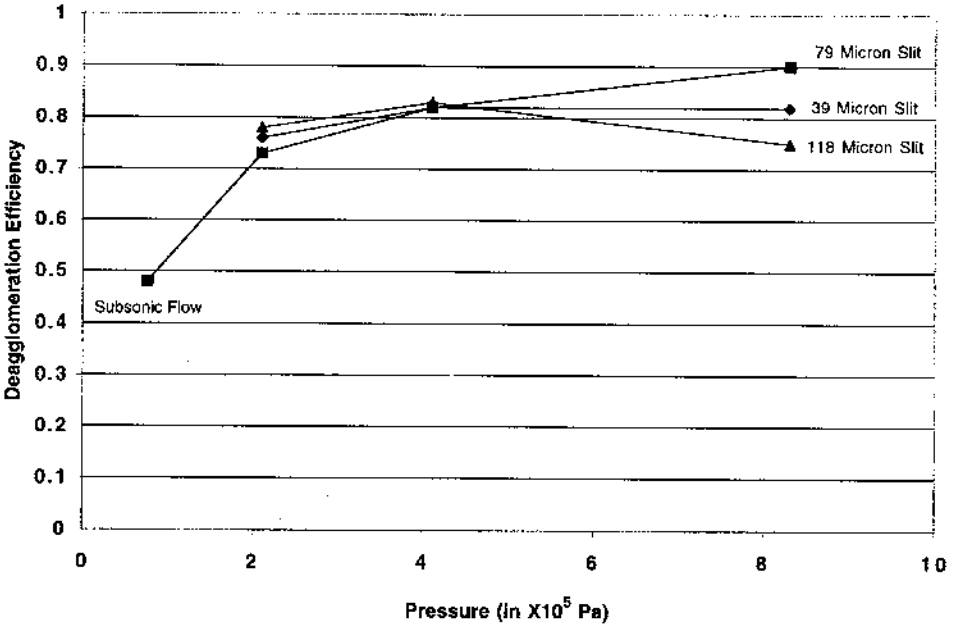

FIGURE 10. Deagglomeration efficiency versus pressure for three slit widths and $Ln(I/I0) = 5$.

diameter glass beads at the settings used for the repeated tests with the Arizona dust described above. Both the concentration achieved and the degree of deagglomeration achieved with the glass microspheres fall within the scatter and uncertainty of the dust data points.

Scanning Electron Microscope (SEM) photographs of example deagglomerated test dust samples are shown in Figure 11.

LOW-G TESTS

NASA facilities offer both suborbital (drop towers), aircraft (KC-135), and orbital (space shuttle) vehicles as platforms for low-g experimentation. Fundamental aerosol physics experiments would in some cases benefit from reduced gravity, which would allow the study of particle-particle and particle-gas interactions in the absence of sedimentation (Huntington et al. 1994). One example of a process which would so benefit is the coagulation of micrometer-sized or larger particles; such coagulation processes are widely relevant to disciplines including earth's atmospheric aerosol studies, planetary formation and atmospheres, and the accumulation of carbonaceous material in space. Since low-g experimentation in principle allows the elimination of both particle sedimentation and differential velocities, there is continued interest in low-g coagulation experiments. Proof-testing of the deagglomerator in brief low-g flights was conducted as a means of verifying that the method is truly gravity independent.

NASA's KC-135 research aircraft, based at Johnson Space Center (Ellington Field) near Houston, TX, is often flown in a series of 30–40 ascending and descending parabolic trajectories, which provide about 15–20 s of "low-g" during each parabola. During this time, the g-level is reduced to about 10^{-2} of the standard value. These experiment times were generally insufficient for the study of coagulation processes, but they did allow thorough perfor-

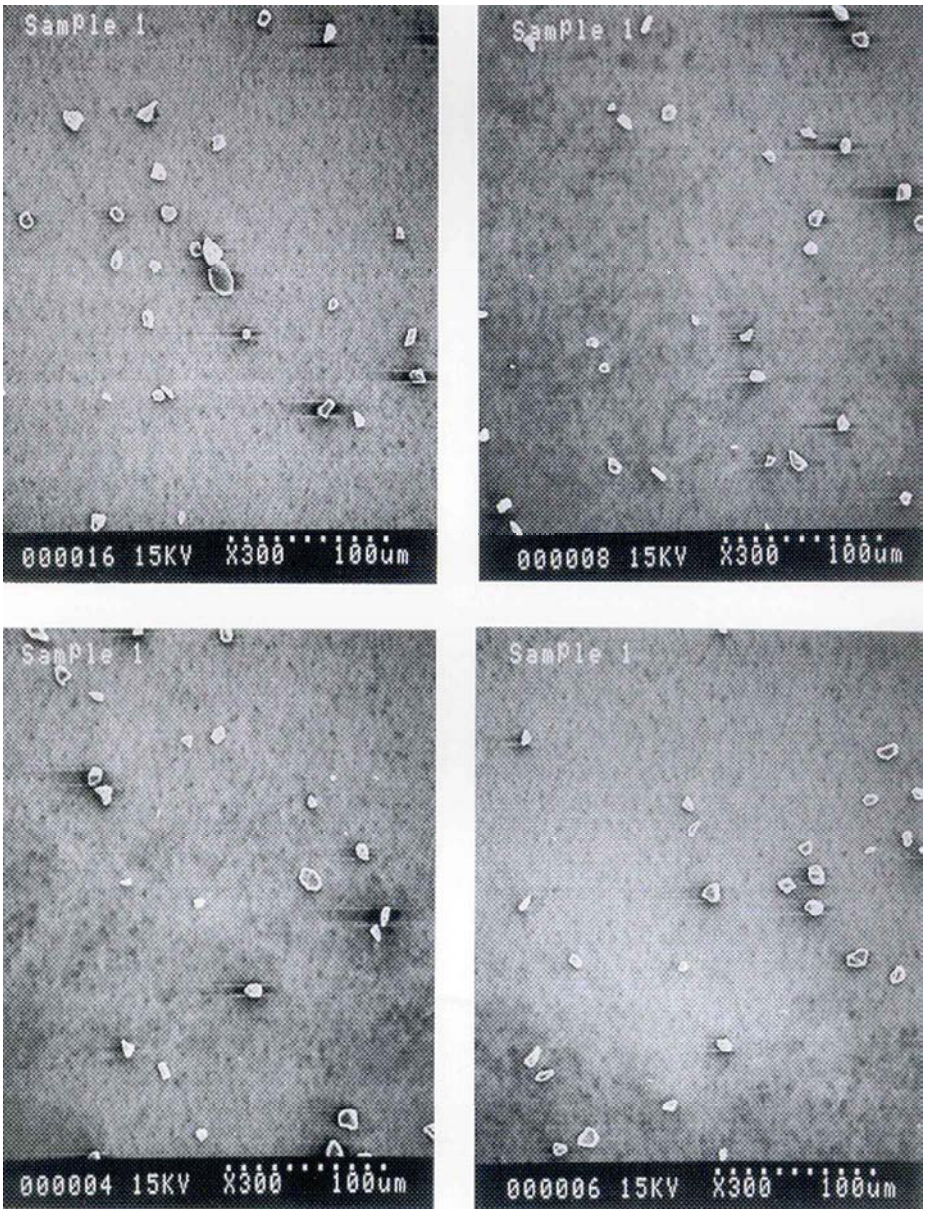

FIGURE 11

mance checks of the deagglomerator system and its efficiency. The deagglomerator and experiment chamber were repackaged in an experiment testbed which met the structural and safety requirements of the KC-135 platform (Figure 12). The deagglomerator was mounted onto one sidearm of a "T"-shaped chamber of approximately 51 L in volume. Deagglomerated and dispersed particles were sampled on 13-mm Nuclepore (Costar, Inc., Cambridge, MA)

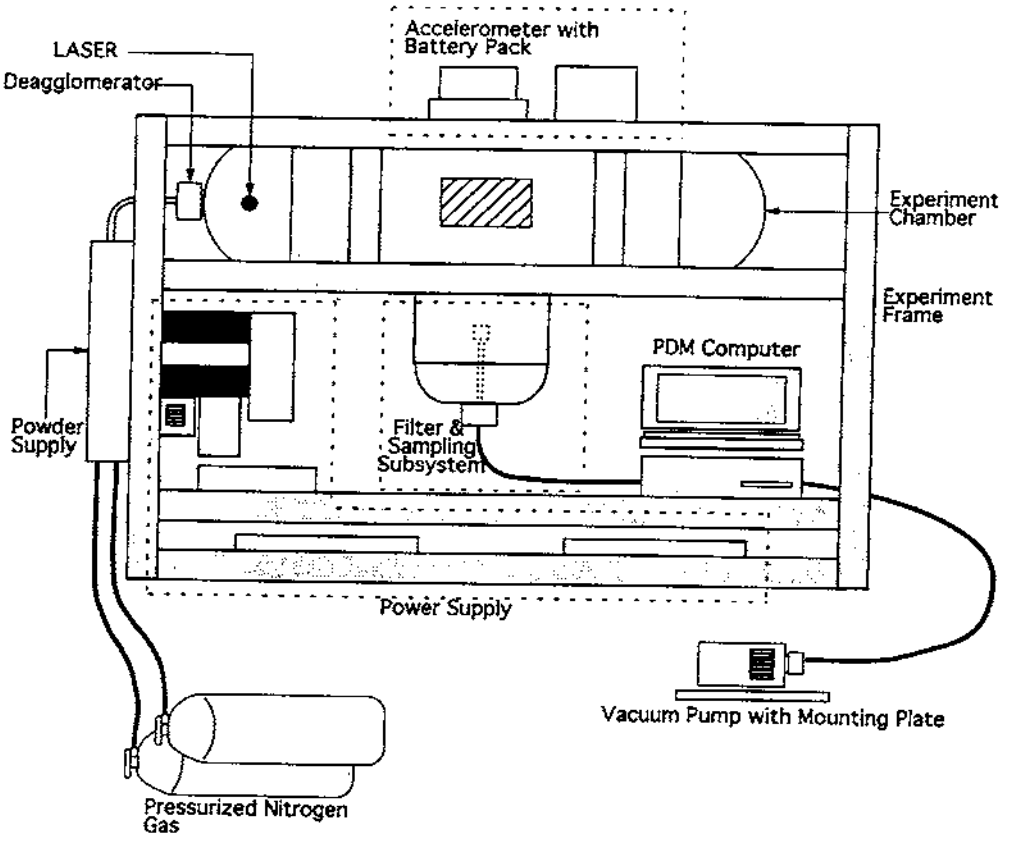

FIGURE 12. Particle dispersion module.

filter media inserted into the center section of the tee using a 1 cm^3/s flow rate. The system was operated under microprocessor control, including the deagglomerator and filter sampling operations; however, the powder sample holders required manual changing between parabolas. Future experiments will utilize two deagglomerators, one operating from each end of this chamber, allowing the use of two different particle types or doubling of the concentrations of a single type. This testbed is available for use by interested scientists.

During three flight sequences in October, 1994, repeated deagglomerator tests were performed on the KC-135 utilizing nearly monodispersed 5–10 μm Arizona test dust identical to the one-g lab tests. Dust masses of 40, 80, and zero (blank) milligrams were used. The dilution and push pressure settings covered the same range as the choked-flow laboratory tests, 4.1 to 8.3×10^5 Pa. The 13 mm filters were recovered and examined by SEM. Table 2 shows deagglomeration efficiencies based on the SEM data from several example experiments computed

TABLE 2. KC-135 Test deagglomeration efficiencies: Combined day 2 results based on SEM photos.

Filter ID	Dust Mass (mg)	Slit Width (μm)	Dilution Pressure (Pa)	Push Pressure (Pa)	Singlet Count (N1)	Doublet Count (N2)	Triplet Count (N3)	Efficiency (Equation 2)
21,23	40	80	8.3×10^5	8.3×10^5	116	4	1	0.87[1]
28,30,32	80	80	6.6×10^5	4.1×10^5	165	8	1	0.90

[1]One seven-member agglomerate was found in one view on one filter in this series. No other agglomerates with more than three members were found on any of the other filters in these experiments.

according to Equation (2). These results constitute performance checks of the deagglomerator in low-g and are equal, within uncertainties, to the efficiencies shown in Table 1 for one-g operation.

SUMMARY

The deagglomerator system was characterized by one-g and low-g tests using 5–10 μm dry mineral dust particles. In addition, one-g tests were conducted using 10.2 and 2.1 μm glass microspheres. One-g deagglomeration data were obtained for the dust particles at 2.1, 4.1, and 8.3 $\times$ 10^5 Pa (30, 60, and 120 psig) operating pressures, and with 39, 79, and 118 μm slit widths. Concentrations were varied over the range from about 1×10^{-4} g/cm^3 to about 1.5×10^{-3} g/cm^3. Additional data were obtained at 7.6×10^4 Pa (11 psig) to investigate the effect of using unchoked flow. Replicate tests were included.

Deagglomeration efficiencies fall in the range from 40 to 94% for the one-g tests with mineral dusts; efficiencies exceed 90% when the dilution flow and dust mass are optimal (Table 1). Low-g test efficiencies, using mineral dust, are estimated to fall in the range from about 80 to 90%. The repeatability of the deagglomeration efficiencies is approximately $\pm$ 10%. The critical controlling parameter in this aerodynamic deagglomerator configuration (apart from particle size) is the peak concentration (particle mass/carrier gas volume) of the material injected into the deagglomerator. The addition of a dilution flow allows control of the particle concentration. The main developments and findings of this investigation are that deagglomerator performance enhancement and dilution control have been added to a previously existing concentric cone design; a quantitative deagglomeration efficiency evaluation methodology has been developed, based on systematic application of a test parameter matrix; deagglomeration efficiencies (singlet particles, Equation (2)) of > 90% are attainable with careful control of powder concentrations; the deagglomerator system performance is gravity independent; and the low-g test facility is available for use by the scientific community.

The authors would like to acknowledge additional guidance and important contributions from the following key individuals in contributing to the successful NASA KC-135 flight and post flight data analysis. Combined efforts from individuals included Michael Meyer (Space Sciences NASA Headquarters), Linda Billica (Ellington Field Texas), Jim Zamel (TRW Space and Technology Electronic Group), Tony Briceno, Jeff Jenner, David Blake, and Bruce Borchers (NASA Ames Research Center), John Marshall, Kathy Kato, and Maureen Savage (SETI Institute).

References

Eadie, F. S., and Payne, R. E., (1954). Particle Size Distribution Analyzed Quickly, Accurately, *Iron Age* 10:99–102.

Fuchs, N. A. (1989). *The Mechanics of Aerosols*, Dover Publications, Mineola, NY.

Fuchs, N. A., and Murashkevich, F. I. (1970). Laboratory Powder Disperser (Dust Generator), *Staub-Reinhalt. Luft* 11:1–3.

Fuchs, N. A., and Selin, A. N. (1964). Pneumatic Dispersion of Powders, *Ingenerno-Fizicheskii Zh.* 7:122–126.

Hidy, G. M. (1984). *Aerosols*, Academic Press, Orlando, FL.

Hinds, W. C. (1980). *Aerosol Technology*, John Wiley and Sons, New York.

Huntington, J. L., Greenwald, K., Rogers, C. F., Stratton, D. M., Simmons, B., and Fonda, M. L. (1994). *Gas-Grain Simulation Facility: Aerosol and Particle Research in Microgravity*, National Aeronautics and Space Administration Conference Publication 10135.

Iinoya, K., and Masuda, H. (1980). Experimental Study on the Dispersion of Fine Particles Into Air. In *Generation of Aerosols and Facilities for Exposure Experiments*, edited by K. Willeke. Ann Arbor Science Publishers Inc., Ann Arbor, MI, pp. 189–202, Chapter 9.

John, W. (1993). The Characteristics of Environmental and Laboratory-Generated Aerosols. In *Aerosol Measurement, Principles Techniques and Applications* , edited by K. Willeke and P. A. Baron. Van Nostrand Reinhold, New York, pp. 54–76, Chapter 5.

Pinnick, R. G., and Rosen, J. M. (1979). Response of Knollenberg Light-Scattering Counters to Non-Spherical Doublet Polystyrene Latex Particles, *J. Aerosol Sci.* 10:533–538.

Rajathurai, A. M., Roth, P., and Fissan, H. (1990). A Shock and Expansion Wave-Driven Powder Disperser, *Aerosol Sci. Technol.* 12:613–619.

Twomey, S. (1977). *Atmospheric Aerosols*, Elsevier Scientific Publishing Company, New York.

Received September 10, 1997; accepted December 14, 1998.